MR Imaging and Spectroscopy Using Hyperpolarized ^{129}Xe Gas: Preliminary Human Results

John P. Mugler III, Bastiaan Driehuys, James R. Brookeman, Gordon D. Cates, Stuart S. Berr, Robert G. Bryant, Thomas M. Daniel, Eduard E. de Lange, J. Hunter Downs III, Christopher J. Erickson, William Happer, Denise P. Hinton, Neal F. Kassel, Therese Maier, C. Douglas Phillips, Brian T. Saam, Karen L. Sauer, Mark E. Wagshul

Using a new method of xenon laser-polarization that permits the generation of liter quantities of hyperpolarized ^{129}Xe gas, the first ^{129}Xe imaging results from the human chest and the first ^{129}Xe spectroscopy results from the human chest and head have been obtained. With polarization levels of approximately 2%, cross-sectional images of the lung gas-spaces with a voxel volume of 0.9 cm^3 (signal-to-noise ratio (SNR), 28) were acquired and three dissolved-phase resonances in spectra from the chest were detected. In spectra from the head, one prominent dissolved-phase resonance, presumably from brain parenchyma, was detected. With anticipated improvements in the ^{129}Xe polarization system, pulse sequences, RF coils, and breathing maneuvers, these results suggest the possibility for ^{129}Xe gas-phase imaging of the lungs with a resolution approaching that of current conventional thoracic proton imaging. Moreover, the results suggest the feasibility of dissolved-phase imaging of both the chest and brain with a resolution similar to that obtained with the gas-phase images.

Key words: hyperpolarized ^{129}Xe; MRI of lung; MRS of lung; MRS of brain.

INTRODUCTION

Recent research has demonstrated the feasibility of performing magnetic resonance imaging and spectroscopy using laser-polarized ^{3}He and ^{129}Xe gases (1–9). Laser optical pumping (10) increases the nuclear spin polarization above thermal equilibrium by several orders of magnitude, yielding hyperpolarized gases with polarizations on the order of tens of percent. The increased polarization more than offsets the spin density difference between the gaseous and liquid states, enabling high-resolution imaging of gas spaces such as the lungs (1–3, 5–9).

While gas-space imaging is possible using both ^{3}He and ^{129}Xe, the solubility of xenon in blood and lipid-rich tissue (11) presents the attractive possibility of dissolved-phase imaging. Xenon-MRI may allow perfusion imaging of the brain, lung, or other regions. Combined imaging of the gas-phase and dissolved-phase xenon would provide a high-resolution, cross-sectional ventilation/perfusion study of the lung (1). Since the solution-phase resonances of xenon are shifted by approximately 200 ppm from the gas-phase resonance (12), it may be feasible to collect both gas and dissolved-phase ^{129}Xe images within a single rapid acquisition.

Although ^{129}Xe spectroscopy and imaging of relatively small volumes (1, 4, 6, 7) have been performed, spectroscopy or imaging of larger volumes, namely the human lungs and brain, has not been possible because methods for generating sufficient quantities of hyperpolarized xenon did not exist. In this communication, we present the first results obtained using a new method for xenon laser-polarization that provides liter quantities of hyperpolarized gas.

METHODS

Preparation and Delivery of the Hyperpolarized Gas

The high-volume production method of laser-polarized ^{129}Xe is described in detail elsewhere (13). Briefly, in a flowing gas stream of 1% Xe, 1% N_2, and 98% ^{4}He, ^{129}Xe is polarized via spin exchange with an optically pumped rubidium (Rb) vapor. Approximately 100 watts of circularly polarized light centered at 795 nm from a diode laser array (Optopower Corp., Tuscon, AZ) is used to excite the Rb D1 absorption resonance. The flow rate is set such that a given ^{129}Xe atom spends 1–2 spin exchange time constants in contact with the polarized Rb vapor. Upon exiting the pumping chamber, the hyperpolarized xenon gas is trapped as a solid in a cold finger surrounded by liquid nitrogen. Under suitable circumstances, the polarization is substantially retained during freezing (14), and the T_1 relaxation time of solid ^{129}Xe at 77 K is approximately 3 h in a magnetic field of 50 mT or more (15). The final polarization of the ^{129}Xe is a function of the accumulated volume of gas, the gas flow rate, and the accumulation time. Calculations show that 500 cm^3 of ^{129}Xe with a polarization of 60% can be accumulated in 1.4 h using a xenon flow rate of 6 cm^3/min (13).

Hyperpolarized ^{129}Xe was accumulated for each experiment over a period of 1–2 h. Enriched xenon gas (71% ^{129}Xe) was obtained from Urenco, Almelo, the Netherlands, and the He-Xe-N_2 gas mixture was then prepared by Isotec, Inc., Miamisburg, OH. When a given accumulation run was finished, the frozen xenon was sublimed and collected in a small plastic bag equipped with a

MRM 37:809–815 (1997)

From the Departments of Radiology (J.P.M., J.R.B., S.S.B., E.E.D., C.D.P.), Chemistry (R.G.B.), Surgery (T.M.D.),Neurosurgery (J.H.D., N.F.K.), Cardiology (D.P.H.) and Engineering Physics (T.M.), University of Virginia Health Sciences Center, Charlottesville, Virginia; the Department of Physics (B.D., G.D.C., C.J.E., W.H., B.T.S., K.L.S.), Princeton University, Princeton, New Jersey; and the Department of Radiology (M.E.W.), State University of New York at Stony Brook, Stony Brook, New York.

Address correspondence to: John P. Mugler III, Ph.D., Department of Radiology, Box 170, HSC, University of Virginia, Charlottesville, Virginia 22908.

Received November 12, 1996; revised February 18, 1997; accepted February 19, 1997.

The development of the xenon-polarization system was supported by AFOSR, ARO, and DARPA. The MR imaging and spectroscopy experiments were supported by the University of Virginia Pratt Fund, the Dean of the Medical School, Dr. Robert M. Carey, and Siemens Medical Systems.

0740-3194/97 $3.00

Copyright © 1997 by Williams & Wilkins
All rights of reproduction in any form reserved.

hand-operated valve (Jensen Inert Products, Coral Springs, FL) for transport to the imager, where the volunteer was already positioned in the magnet. The T_1 of the hyperpolarized ^{129}Xe gas in the bag was approximately 10 min. The volunteer inhaled between 300 and 500 cm^3 of gas from the bag through a plastic tube, either in one large breath (six of seven experiments) or in four small incremental breaths (one experiment). In the case of one large breath, imaging or spectroscopy commenced immediately after gas inhalation. In the case of four small breaths, data collection continued throughout the breathing period.

The polarization achieved during each accumulation run was calculated by comparing the free-induction decay signal recorded from a 5-cm^3 glass bulb filled with a sample of hyperpolarized xenon gas to that recorded from a similar glass bulb filled with xenon gas at thermal spin equilibrium. These measurements were made using a 4.7 T, 40-cm bore imager/spectrometer (Varian Associates, Palo Alto, CA). For the reported experiments, the estimated polarizations ranged from 0.1–2.7%. These polarization values are substantially lower than the theoretically predicted value given above. However, these values represent the results from the first application of the prototype polarization system.

Imaging and Spectroscopy Procedures

Three healthy volunteers (two male and one female, mean age 25 years) participated in seven experiments. These included coronal lung images (two subjects), axial lung images (one subject), chest spectra (two subjects), and head spectra (one subject, two sessions).

All imaging and spectroscopy experiments were performed using a 1.5 T commercial whole-body imager (Magnetom Vision, Siemens Medical Systems, Iselin, NJ). This instrument was modified to operate at 17.6 MHz by the addition of a broadband RF amplifier and a ^{129}Xe volume RF coil. The RF coil was a modified commercial (Siemens) 1.5 T sodium head coil (transmit/receive, linearly polarized). A capacitor was removed from the tuning circuit, which allowed the coil to be tuned to the xenon frequency. The inside diameter of the coil was 29 cm, which was large enough to accommodate the chest of a slim adult. Due to the different coil loading for the chest compared with the head, we were only able to tune the coil to be 85% efficient (15% reflected power) with an adult chest in the coil. With an adult head in the coil, we were able to tune the coil to be 100% efficient. For imaging or spectroscopy of the chest, the coil was positioned over the lungs with one end at the level of the shoulders and the opposite end over the abdomen. For spectroscopy of the head, the coil was positioned with one end just below the chin and an RF-opaque blanket (a standard accessory for our imager) was wrapped around the chest. This was done to minimize the excitation of hyperpolarized gas in the lungs while collecting spectra from the head to minimize reception of signals from the chest.

Typical prescan procedures were omitted to prevent depolarization of the nonequilibrium ^{129}Xe magnetization (5, 8, 9). Instead, resonant frequency selection, transmitter output calibration, and receiver gain settings were performed beforehand using a small glass bulb or a plastic bag filled with hyperpolarized gas. With the glass bulb placed on the chest or in the mouth of the volunteer, the resonant frequency was selected based on the signal obtained after a single hard RF pulse. Using the same configuration, the transmitter calibration was estimated based on the signal amplitudes recorded after each of 10–15 consecutive hard RF pulses of equal (but unknown) flip angles, spaced approximately 5 s apart. Neglecting T_1 relaxation, the ratio of consecutive signal amplitudes equals the cosine of the flip angle. Approximately 10 signal ratios were averaged to determine the calibration relating the transmitter output to the flip angle. The receiver gain setting was determined based on the signal received from the plastic bag filled with approximately 500 cm^3 of hyperpolarized gas. The frequency and transmitter calibrations were performed once per volunteer and the receiver calibration was performed once for all experiments.

Images of the lungs were acquired using a two-dimensional low-flip angle gradient-echo pulse sequence (FLASH) with the following parameters: *TR/TE* 190 ms/5.6 ms, flip angle 9° (sequential phase encoding) or 12° (centric phase encoding), matrix size 64 × 128, voxel size 6.6 × 13.3 × 20 mm or 6.6 × 6.6 × 20 mm, and NEX 1. Eleven contiguous sections were collected during a 12-s breath-hold. Estimating that the acquisition reduces the initial magnetization by a factor of $\cos^n\alpha$ (n = number of phase encoding steps and α = flip angle), the sequential and centric phase-encoding acquisitions used 55% ($1 - \cos^{64}9°$) and 76% ($1 - \cos^{64}12°$) of the available magnetization, respectively. (This estimate neglects any diffusion-driven exchange of the magnetization between sections.) For coronal image sets, corresponding proton images were acquired using a low-flip angle FLASH sequence and the body RF coil. The proton images were obtained immediately after the xenon images, leaving the xenon RF coil, and hence the subject, in the same position. The signal-to-noise ratios (SNR) for the xenon images were calculated from region-of-interest measurements.

Free induction decays were collected from the chest using the following parameters: 250 μs, 10° hard RF pulse, 51.2 ms data sampling period (19.5 Hz frequency resolution), and 512 complex points. There was a 1-ms delay between the end of the RF pulse and the beginning of data acquisition to prevent signal contamination from transmitter ring-down. An FID was collected every second for 128 repetitions, commencing just after inhalation of the hyperpolarized gas, continuing throughout the breath-hold period and into quiet respiration. The FIDs were transferred to the 4.7 T system (described above) for processing. The FIDs were zero-filled to 2048 points, apodized by multiplication with an exponential (25 Hz for Fig. 2, 8 Hz for Fig. 3), and Fourier transformed. A zero-order phase correction was applied to all spectra. To improve our ability to resolve the dissolved-phase peaks from the chest, spectra were also processed to remove the large, broad gas peak by applying a bandpass digital filter (2500 Hz [140 ppm] bandwidth, centered on the gas peak) and then subtracting the unfiltered spectra.[1] From the spectra, the peak positions of the

[1] Low-frequency solvent-subtraction filtering, Chapter 5, System Operation Manual, VNMR Version 5.3 Software, Varian Associates, Palo Alto, CA, 1996. Except as noted above, default filter parameters were used.

dissolved components relative to the gas resonance and the integrals of the dissolved components were calculated.

Free induction decays were collected from the head using the following parameters: 600 μs, 90° hard RF pulse, 51.2 ms data sampling period, and 512 sample points. As before, a 1-ms delay was inserted between the end of the RF pulse and the beginning of data acquisition. In one of the experiments, an FID was collected every 10 s for 16 repetitions. In the other experiment, an FID was collected every 5 s for 32 repetitions. In both cases, data acquisition commenced just after inhalation of the hyperpolarized gas and continued throughout the breath-hold period and into quiet respiration. The FIDs were processed as outlined in the previous paragraph (apodization 25 Hz for Fig. 4), except that no digital filtering was applied and the results are displayed as magnitude spectra.

The xenon MR protocols were approved by our institutional review board and informed consent was obtained from all volunteers. Throughout each experimental session, the subject's heart rate and blood oxygen saturation were monitored. All procedures were supervised by one of our staff radiologists.

RESULTS AND DISCUSSION

Side Effects from Inhaled Xenon

No unusual variations in the heart rate and blood oxygen saturation of the volunteers were noted. However, in one experiment, the volunteer experienced some slight side effects (numbness in the legs, nausea) commonly associated with anesthesia. Based on the known properties of xenon, the possibility of such side effects was recognized before the experiments and was listed in our consent form. Other effects reported by the volunteers included a floral aroma and a slight feeling of euphoria.

Lung Gas-Space Images

In all three imaging experiments, the full extent of the left and right lungs was depicted, with the exception of the most superior portions of the lungs, which extended past the end of the RF coil. The axial image sections and the central sections of the coronal image sets demonstrated relatively well-defined edges at the lung surfaces. (The more anterior and posterior coronal images demonstrated less defined edges presumably due to the curvature of the lung surface, partial volume averaging, and the relatively thick [2 cm] sections.) In two of the image sets, signal was also apparent in the trachea. For the other image set, the volunteer was instructed to take a small gulp of air after inhalation of the hyperpolarized gas, thereby clearing the ^{129}Xe from the trachea. The maximum SNRs for the three xenon image sets were 32 (1.8 cm^3 voxel, centric phase encoding), 9 (1.8 cm^3 voxel, sequential phase encoding), and 28 (0.9 cm^3 voxel, centric phase encoding).

Figure 1 shows three contiguous coronal xenon lung images, as well as corresponding proton images, from one of the three imaging experiments. Comparing the xenon and proton images, good correlation is seen between the gas-space signal void in the proton images and the gas-space signal in the xenon images, although an exact correspondence is not expected since the xenon and proton images were acquired in two separate breath-hold periods.

In each experiment, several of the images demonstrated regional signal intensity variations. However, because the sample size is small and the breathing maneuvers were not carefully controlled in these preliminary studies, we are hesitant to draw a conclusion regarding the significance of these observed intensity variations. An interesting possibility is that the heavy xenon gas initially collected in preferred portions of the lung.

Slight ghosting artifacts were apparent in some of the coronal images (centric phase-encoding order) for both volunteers, but not in any of the axial images (sequential phase-encoding order). (For the xenon images in Fig. 1, these ghosting artifacts are just above the noise level and are thus not clearly depicted with image window and level settings appropriate for displaying the lungs.) We believe that these artifacts were caused by bulk mixing of the (heavier) xenon gas with the other lung gases just after inhalation. The low spatial frequencies for all sections are collected in the beginning of the centrically phase-encoded acquisition and in the middle of the se-

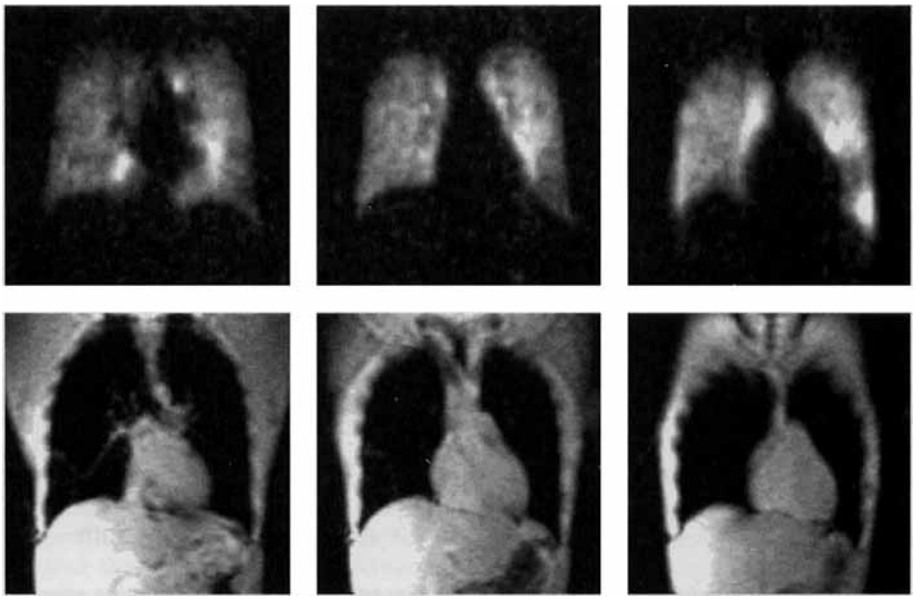

FIG. 1. Contiguous coronal ^{129}Xe lung images (upper panels) and corresponding ^{1}H images (lower panels) of a healthy human volunteer. Good correlation is seen between the gas-space signal void in the proton images and the gas-space signal in the xenon images. See text for pulse sequence parameters.

quentially phase-encoded acquisition. Thus, any signal intensity variations secondary to gas mixing just after inhalation would corrupt low spatial frequencies only for the centric phase-encoding order, resulting in more severe artifacts from motion occurring early in the acquisition. The centric phase-encoding order also results in a low-pass *k*-space filter since the hyperpolarized magnetization is gradually depleted throughout the acquisition. This would result in some degree of blurring, but not ghosting. Variable flip angle strategies (16) could be used to prospectively control the evolution of the magnetization during the acquisition, and hence the degree of image blurring.

The xenon images showed some lung structure, although less than that recently demonstrated with hyperpolarized ^{3}He imaging of the lungs (5, 9). The principal reason for this difference is the factor of 5 increase in the in-plane voxel dimension for the xenon images compared with the helium images because of the lower available signal. Several factors contribute to the large signal level difference between the ^{129}Xe and ^{3}He experiments: 1) gas polarization values were typically 5–20 times lower for the xenon images, 2) inhaled gas volumes were 1.5–3 times lower for the xenon images, and 3) the gyromagnetic ratio for ^{129}Xe is 2.8 times lower than that for ^{3}He.

For the imaging parameters used in our experiments, the dissolved-phase image would be shifted in position approximately one-third of the field-of-view along the readout direction due to the ~200 ppm chemical shift between the gas and dissolved phases of xenon. This large position shift, combined with the large field-of-view, would result in a dissolved-phase image completely separated from the gas-phase image. Since no dissolved-phase image was apparent, presumably due to an insufficient dissolved-phase signal level, we looked for dissolved-phase signals in one-dimensional spectra.

Chest Spectra

The spectra from the two volunteers demonstrated a large peak from the gas phase and three smaller, closely spaced peaks from the dissolved phase, shifted approximately 200 ppm from the gas peak. The chemical shifts, which were measured relative to the gas peak and which varied slightly among spectra for a given volunteer, were 185–186, 195–196, and 216 ppm for the first volunteer and 182–183, 195–196, and 216 ppm for the second volunteer.

Figure 2 presents 25 consecutive spectra from the chest of the first volunteer, showing the temporal evolution of the gas-phase and dissolved-phase signal components. The discontinuity seen in the temporal evolution of the gas phase at the 18th spectrum corresponds to the end of the breath-hold period. Figure 3 shows 60 consecutive spectra from the chest of the second volunteer, demonstrating the temporal evolution of the gas-phase signal component during a four-breath maneuver. For each breath, a portion of the hyperpolarized ^{129}Xe was inhaled, followed by a breath-hold period lasting approximately 10 s. During the exhalation/inhalation period between the second and third breath-holds, a slightly shifted gas peak appears, possibly attributable to a portion of the gas experiencing a bulk magnetic susceptibility frequency shift (7). Less pronounced effects are seen between the first and second, and third and fourth breath-holds.

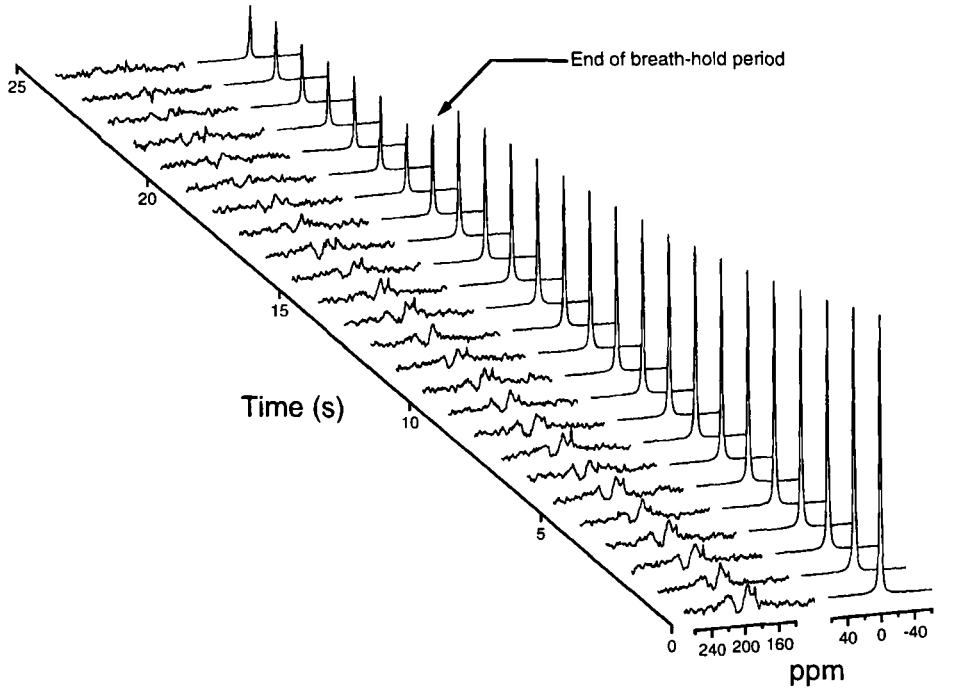

FIG. 2. Twenty-five consecutive ^{129}Xe spectra (one spectrum per second) from the chest of a healthy human volunteer, showing the temporal evolution of the gas-phase and dissolved-phase signal components during and after a 16-s breath-hold period. Data acquisition began immediately after gas inhalation. Peaks at approximately 185, 196, and 216 ppm can be resolved in the dissolved-phase spectra. (The vertical scale for the dissolved-phase spectra is magnified by a factor of 10 compared with that for the gas-phase spectra.)

From the gas-phase signal decays recorded during the breath-hold periods for the two volunteers, we estimate that the apparent T_1 value for this signal component is 22 s for the first volunteer and 16 s for the second volunteer. Among the major factors contributing to the decay of the gas-phase signal are presumably exchange of xenon with blood and lung tissue, and relatively rapid T_1 relaxation due to the presence of oxygen.

The dissolved-phase portion of the spectra shown in Fig. 2 appears very similar to that for a rat thorax shown in Fig. 1a of ref. 6, except that the least-shifted peak of the latter is much higher. Nonetheless, the ratio of the dissolved-phase peak amplitudes to the gas-phase peak amplitude was much smaller for our human

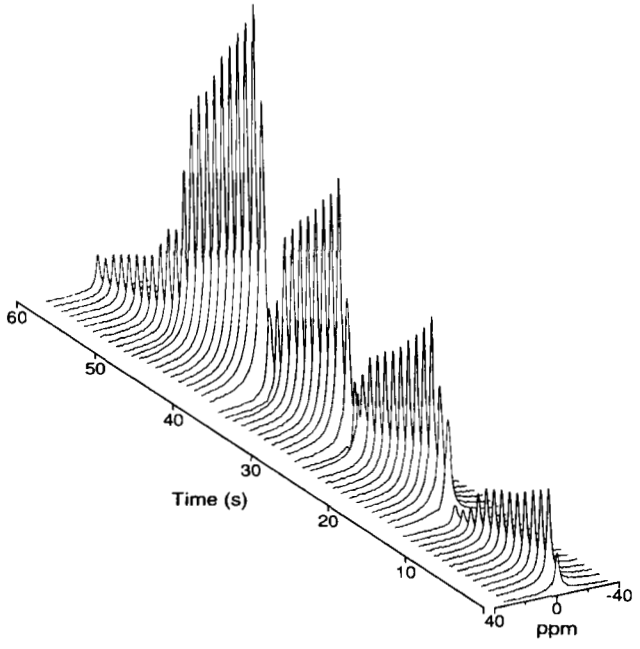

FIG. 3. Sixty consecutive ^{129}Xe spectra (one spectrum per second) from the chest of a healthy human volunteer, demonstrating the temporal evolution of the gas-phase signal component during a four breath-hold maneuver.

studies than for previous animal studies. We expect that the combination of several factors may have played a significant role in producing this difference. These factors include the substantially larger volume (relative to the lung capacity) of xenon inhaled in the animal experiments, the administration of this larger volume of xenon in a manner that presented hyperpolarized gas to the lungs over a considerably greater number of cardiac cycles, and the higher heart rate of the animals. Further investigations will be required to sort out the relative contributions of the volume of xenon inhaled, breathing maneuvers, interspecies differences, and other factors.

The detection of three dissolved peaks from the human chest is consistent with previous results from both rats (6) and mice (7). In comparing the chemical shifts of the peaks, our results are fairly similar to those of ref. 6. In comparing with ref. 7, no peaks beyond 200 ppm were observed, whereas we observed a peak at 216 ppm. Minor differences in peak locations among these results may be due, in part, to bulk magnetic susceptibility effects, and in particular note that our frequency reference was with respect to the gas in the lungs, as opposed to gas outside the subject. With regard to the absence of the 216 ppm peak in the mouse results, preliminary *in vitro* experiments comparing mouse and human blood (private communication, A. Wishnia, M. E. Wagshul, State University of New York at Stony Brook) have revealed the same discrepancy, a peak at approximately 216 ppm is present in the human blood spectrum but absent in that for mice. A possible explanation is that the exchange rate for xenon across the mouse red blood cell membrane is substantially faster than that for human red blood cells.

In previous studies (6, 7), differences between the temporal dynamics of the peaks were seen and were used to help determine the possible sources of the various signal components. In our results, the temporal changes in the integrated intensities of the dissolved peaks correlated, in general, with those of the gas peak. We could not detect any accumulation effects as seen previously (6, 7). However, our breathing maneuvers were different, and the total volume of xenon inhaled was less then 1/10 of the total lung capacity compared with typically many times the lung capacity in the animal studies. In addition, the low SNR and low resolution of the dissolved spectra in our study hindered the temporal analysis. For the four-breath experiment (second volunteer), the SNR of the dissolved peaks was too low to permit the temporal course of the peaks to be followed throughout the experiment.

Assuming previously identified peak assignments, the most-shifted peak in our chest spectra, at 216 ppm, would be from red blood cells. The resonance from red blood cells was detected at 216 ppm in two *in vitro* studies (17, 18) and (putatively) at 213 ppm (also the most-shifted peak) in an *in vivo* study of the rat thorax (6). The peak at 195–196 ppm is consistent with what was assigned as lung parenchyma at 195 ppm (7) or 199 ppm (6). Our least-shifted peak is several ppm lower than any previously reported peak. The least-shifted peaks in previous *in vivo* studies were either assigned to plasma (191 ppm (6)) or well-vascularized tissues in the thorax such as the heart (190 ppm (7)).

Head Spectra

The head spectra demonstrated one peak from the gas phase and one prominent peak from the dissolved phase,

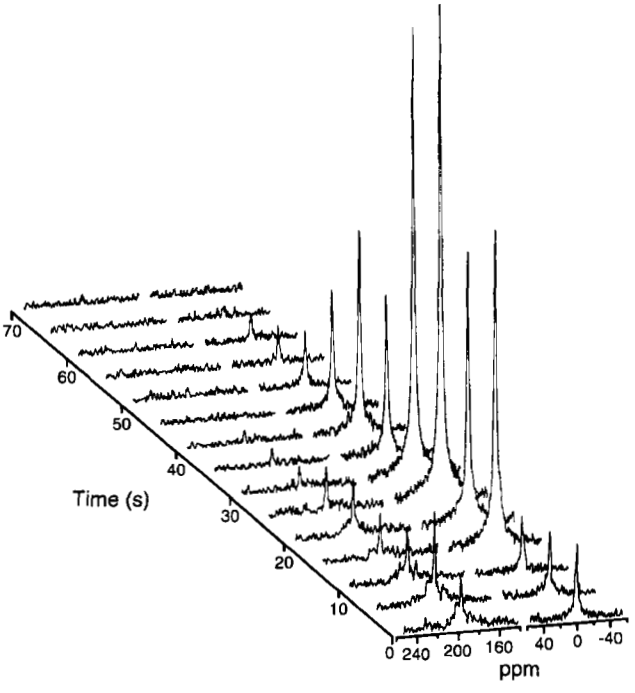

FIG. 4. Fifteen consecutive ^{129}Xe spectra (one spectrum each 5 s) from the head of a healthy human volunteer, demonstrating the temporal evolution of the gas-phase and dissolved-phase signal components during and after a 15-s breath-hold period.

shifted 196 ppm from the gas peak. Presumably, the gas-phase signal came from residual gas in the mouth and trachea and, perhaps, from gas in the most superior portions of the lungs. The absolute frequency of the gas-phase peak was within 1 ppm of that for the gas-phase peaks in the lung spectra. In several spectra, there was an apparent broadening of the lower portion of the 196-ppm peak, potentially indicating a second component at approximately the same chemical shift.

Figure 4 shows 15 consecutive spectra from the head, illustrating the temporal evolution of the gas-phase and dissolved-phase signal components. Decay of the gas-phase signal is seen during the breath-hold period (first three spectra). The gas-phase peak oscillates in amplitude over the next several spectra as gas is expelled from the lungs, through the mouth, and into the air surrounding the coil. The integrated intensities of the dissolved-phase peaks during the first 40 s are plotted in Fig. 5.

In both experiments, a dissolved-phase signal was detected in the first spectrum, collected just at the end of the inhalation period of approximately 5 s. This observation is consistent with the known transit time from the lungs to the brain on the order of 5 s. Since 90° RF pulses were used to acquire the spectra, the observed temporal behaviors reflect the amount of hyperpolarized ^{129}Xe accumulating in the head (brain) during the delays between spectra, modulated by the T_1 decay of polarized gas in the lungs and brain and during transit, and by the depletion of xenon in the lungs. Theoretical models of the transport of hyperpolarized ^{129}Xe to the brain (19) should be useful for understanding the physical and physiological principles underlying the observed temporal evolutions.

The detection of one prominent dissolved peak at 196 ppm is consistent with recent results from rats (private communication, S. D. Swanson, University of Michigan). Considering the relative affinity of xenon for brain tissue as exploited in xenon-enhanced CT (20), we putatively attribute the 196-ppm peak to brain parenchyma. The absence of a red blood cell (216 ppm) peak in the head spectra deserves comment. We postulate that the small volume fraction of blood in the brain, combined with a rapid uptake of xenon by the brain parenchyma, resulted in a blood signal level that fell below the noise level for our experimental conditions.

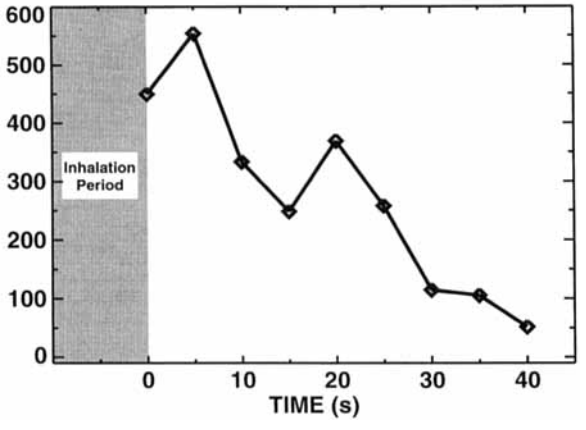

FIG. 5. Integrated intensities of the dissolved-phase peaks shown in Fig. 4 over the first 40 s.

Potential for Dissolved-Phase Imaging

Based on the spectral and image data presented above, we have made a preliminary assessment of the possibility for imaging with the dissolved-phase signal in the chest and head. With respect to the chemical shift of the various dissolved components detected in the chest, we assumed the most favorable situation of a sufficiently high bandwidth per pixel to allow simultaneous imaging of all dissolved components with acceptable chemical shift artifacts. It was also assumed that if the dissolved-phase integrated intensities could be increased to the (present) level of the gas-phase integrated intensity from the chest, then dissolved-phase images of quality and resolution similar to our current gas-phase images would be obtained.

Considering the chest results, the ratio of the gas-phase integral to the sum of the dissolved-phase integrals for the first few spectra shown in Fig. 2 is approximately 300. Within the current state of technology, we believe that the dissolved-phase signal levels can be increased by this factor using the following strategies: 1) Design improvements of the polarization system should permit substantial improvements in the polarization values, approaching those predicted by theory. In the short term, we believe that polarization values for liter quantities of hyperpolarized ^{129}Xe gas can be increased by a factor of 10 to 20–25%. 2) Using a 90° RF excitation pulse, selective for the dissolved resonances so as not to deplete the gas supply for these signals, the transverse magnetization will increase by a factor of 5.8 compared with that generated by a 10° pulse. 3) Assuming the dissolved-phase resonances have T_2 values at least on the order of tens of milliseconds, the use of an echo-train type sequence (e.g., RARE) could allow the total acquisition time per excitation RF pulse to be increased by perhaps a factor of 2 or more, yielding a SNR improvement of $\sqrt{2}$ or more. 4) The RF coil used in the current experiments is a 10-year-old design and was not intended for chest imaging. A dedicated chest-imaging coil based on state-of-the-art technology should provide at least a factor of 2 increase in SNR. 5) Assuming (at least some of) the dissolved-phase resonances are in rapid exchange with the gas phase (6, 7), such that after a spectrally selective 90° RF pulse the dissolved-phase components are replenished in a time period on the order of seconds, it should be feasible to use multiple excitations for the purpose of signal averaging. Four excitations would provide a factor of 2 improvement in the SNR. The product of these factors is 330, suggesting the potential for dissolved-phase imaging of the chest with quality and resolution similar to our current gas-phase images.

Considering the head results, the ratio of the largest gas-phase integral from the chest to the largest dissolved-phase integral from the head is approximately 190. (The dissolved-phase integral was corrected for differences in receiver gain and noise levels between the two experiments.) Strategies 1, 3, 4 (using a state-of-the-art head coil), and 5 discussed in the previous paragraph are also

applicable to dissolved-phase imaging of the head. In addition, assuming the primary signal source is the brain, the volume over which the signal is distributed for head imaging is substantially smaller than that for chest imaging. Assuming the chest volume exceeds that of the brain by at least a factor of 4, the product of all factors is 230, suggesting the potential for dissolved-phase imaging of the brain with quality and resolution similar to our current gas-phase images of the lungs.

Despite the potential suggested by the approach above, it may be advantageous for some applications to instead introduce dissolved-phase xenon directly into blood or tissue using a biologically compatible solvent carrier as recently discussed by Bifone *et al.* (18). Their investigations of xenon dissolved in three different solutions demonstrated that polarization can be preserved during dissolution and that the T_1 in solution was on the order of 10 s or more, suitable for *in vivo* imaging or spectroscopy studies.

As a corollary to the analyses above, note that Strategies 1 and 4 apply equally to gas-phase imaging of the lungs, potentially providing a 20-fold increase in the SNR. This increase could be traded for resolution, yielding a voxel volume of approximately 0.05 cm^3 for an SNR > 20.

CONCLUSIONS

In this study, the first ^{129}Xe imaging results from the human chest and the first ^{129}Xe spectroscopy results from the human chest and head were obtained using a new method for xenon laser-polarization that provides liter quantities of hyperpolarized gas. With maximum polarization levels of approximately 2%, we were able to acquire cross-sectional images of the lung gas-spaces with a voxel volume of 0.9 cm^3 (SNR 28) and to detect dissolved-phase resonances in spectra from the chest. These dissolved-phase spectra demonstrated three peaks, consistent with previous results from rats (6) and mice (7). In spectra from the head, one prominent dissolved-phase resonance was detected. With anticipated technical improvements in the xenon-gas polarization system, polarizations of 20–25% are expected. Such an increase in polarization, considered along with other potential SNR increases from optimized pulse sequence techniques, RF coils, and breathing maneuvers, suggests the potential for gas-phase imaging of the lungs with a resolution approaching that of current conventional proton imaging of the chest and dissolved-phase imaging of the chest and brain with resolution similar to our current gas-phase images.

ACKNOWLEDGMENTS

The authors thank Mike Souza for his expert glassblowing; Joseph Camaratta, Dr. Wilhelm Dürr, Andreas Potthast, and Phillip Belcher for their invaluable assistance in bringing the broadband imaging/spectroscopy option and the xenon RF coil into operation; and John Christopher, RT(R)(MR), Hamish Brookeman, Vu Mai, and Michelle Plantec for valuable assistance with the MR studies.

REFERENCES

1. M. S. Albert, G. D. Cates, B. Driehuys, W. Happer, B. Saam, C. S. Springer, Jr, A. Wishnia, Biological magnetic resonance imaging using laser-polarized ^{129}Xe. *Nature* **370,** 199–201 (1994).
2. H. Middleton, R. D. Black, B. Saam, G. D. Cates, G. P. Cofer, R. Guenther, W. Happer, L. W. Hedlund, G. A. Johnson, K. Juvan, J. Swartz, MR imaging with hyperpolarized ^3He gas. *Magn. Reson. Med.* **33,** 271–275 (1995).
3. R. D. Black, H. L. Middleton, G. D. Cates, G. P. Cofer, B. Driehuys, W. Happer, L. W. Hedlund, G. A. Johnson, M. D. Shattuck, J. C. Swartz, In vivo He-3 MR images of guinea pig lungs. *Radiology* **199,** 867–870 (1996).
4. M. S. Albert, C. H. Tseng, D. Williamson, E. R. Oteiza, R. L. Walsworth, B. Kraft, D. Kacher, B. L. Holman, F. A. Jolesz, Hyperpolarized ^{129}Xe MR imaging of the oral cavity. *J. Magn. Reson. Series B* **111,** 204–207 (1996).
5. J. R. Macfall, H. C. Charles, R. D. Black, H. Middleton, J. C. Swartz, B. Saam, B. Driehuys, C. Erickson, W. Happer, G. D. Cates, G. A. Johnson, C. E. Ravin, Human lung air spaces: potential for MR imaging with hyperpolarized He-3. *Radiology* **200,** 553–558 (1996).
6. K. Sakai, A. M. Bilek, E. Oteiza, R. L. Walsworth, D. Balamore, F. A. Jolesz, M. S. Albert, Temporal dynamics of hyperpolarized ^{129}Xe resonances in living rats. *J. Magn. Reson. Series B* **111,** 300–304 1996.
7. M. E. Wagshul, T. M. Button, H. F. Li, Z. Liang, C. S. Springer, K. Zhong, A. Wishnia, In vivo MR imaging and spectroscopy using hyperpolarized ^{129}Xe. *Magn. Reson. Med.* **36,** 183–191 (1996).
8. P. Bachert, L. R. Schad, M. Bock, M. V. Knopp, M. Ebert, T. Großmann, W. Heil, D. Hofmann, R. Surkau, E. W. Otten, Nuclear magnetic resonance imaging of airways in humans with use of hyperpolarized ^3He. *Magn. Reson. Med.* **36,** 192–196 1996.
9. H. U. Kauczor, D. Hofmann, K. F. Kreitner, H. Nilgens, R. Surkau, W. Heil, A. Potthast, M. V. Knopp, E. W. Otten, M. Thelen, Normal and abnormal pulmonary ventilation: visualization at hyperpolarized He-3 MR imaging. *Radiology* **201,** 564–568 (1996).
10. W. Happer, E. Miron, S. Schaefer, D. Schreiber, W. A. van Wijngaarden, X. Zeng, Polarization of the nuclear spins of noble-gas atoms by spin exchange with optically pumped alkali-metal atoms. *Phys. Rev. A* **29,** 3092–3110 (1984).
11. H. Susskind, K. J. Ellis, H. L. Atkins, S. H. Cohn, P. Richards. Studies of whole-body retention and clearance of inhaled noble gases. *Prog. Nucl. Med.* **5,** 13–34 (1978).
12. K. W. Miller, N. V. Reo, A.J.M.S. Uiterkamp, D. P. Stengle, T. R. Stengle, K. L. Williamson, Xenon NMR: chemical shifts of a general anesthetic in common solvents, proteins, and membranes. *Proc. Natl. Acad. Sci. USA* **78,** 4946–4949 1981.
13. B. Driehuys, G. D. Cates, E. Miron, K. Sauer, D. K. Walter, W. Happer, High-volume production of laser-polarized ^{129}Xe. *Appl. Phys. Lett.* **69,** 1668–1670 (1996).
14. G. D. Cates, D. R. Benton, M. Gatzke, W. Happer, K. C. Hasson, N. R. Newbury, Laser production of large nuclear-spin polarization in frozen xenon. *Phys. Rev. Lett.* **65,** 2591–2594 (1990).
15. M. Gatzke, G. D. Cates, B. Driehuys, D. Fox, W. Happer, B. Saam, Extraordinarily slow nuclear spin relaxation in frozen laser-polarized ^{129}Xe. *Phys. Rev. Lett.* **70,** 690–693 (1993).
16. L. Zhao, R. Mulkern, C. H. Tseng, D. Williamson, S. Patz, R. Kraft, R. L. Walsworth, F. A. Jolesz, M. S. Albert, Gradient-echo imaging considerations for hyperpolarized ^{129}Xe MR. *J. Magn. Reson. Series B* **113,** 179–183 (1996).
17. M. Albert, V. Schepkin, T. Budinger, Measurement of ^{129}Xe T1 in blood to explore the feasibility of hyperpolarized ^{129}Xe MRI, *in* "Proc., SMR, 3rd Annual Meeting, Nice, 1995," p. 1193.
18. A. Bifone, Y-Q. Song, R. Seydoux, R. E. Taylor, B. M. Goodson, T. Pietraß, T. F. Budinger, G. Navon, A. Pines, NMR of laser-polarized xenon in human blood. *Proc. Natl. Acad. Sci. USA* **93,** 12932–12936 (1996).
19. S. Peled, F. A. Jolesz, C. H. Tseng, L. Nascimben, M. S. Albert, R. L. Walsworth, Determinants of tissue delivery for ^{129}Xe magnetic resonance in humans. *Magn. Reson. Med.* **36,** 340–344 (1996).
20. H. Yonas, D. W. Johnson, R. R. Pindzola, Xenon-enhanced CT of cerebral blood flow. *Sci. Am. Sci. Med.* **2,** 58–67 (1995).